New Insights of the Switching Process in GeAsTe Ovonic Threshold Switching (OTS) Selectors

Zeyu Hu, Weidong Zhang, Robin Degraeve, Daniele Garbin, Zheng Chai, Nishant Saxena, Pedro Freitas, Andrea Fantini, Taras Ravsher, Sergiu Clima, Jian Fu Zhang, Romain Delhougne, Ludovic Goux, Gouri Kar

Abstract— **Experimental evidence and analysis in this work provide new insights into the fast-switching process in GeAsTe ovonic threshold switching (OTS) selectors. For the first time, the full switching-off process, covering the defect cluster shrinking and rupture stages, can be measured and characterized. Two distinct switch-off mechanisms and their dependence on the total impedance of the selector and resistor (1S1Rs) circuit are identified. The impact of series resistance value on the switching process, the 1S1Rs operation, and the underlying mechanisms can be explained by the dynamic resistance of OTS that is induced by the transition of defect clusters. This research sheds new light on OTS switching mechanism and its impact on 1S1Rs operation.**

Index Terms—**Ovonic Threshold Switching, OTS, Selector, emerging memory, mechanism, defects, 1S1R.**

I. INTRODUCTION

Selector device plays a key role in suppressing the sneak path currents in the crossbar arrays that utilize the emerging non-volatile memory devices [1, 2], such as the phase change memory (PCRAM) [3], the Redox based and oxide based resistive switching memory (ReRAM/OxRAM) [4]. The selector should have fast volatile switching characteristics when connected in series with the non-volatile memory device. When the memory device is not selected, it is biased at a half of the operation voltage, ½V_{op}, at which the selector should have very low off-state current and can suppress the overall leakage current and avoid the sneak current path. When the memory device is selected at the operation voltage, V_{op}, the selector should be at the ON state and allow a sufficiently high current to pass through, so that the memory device can be programmed. A large on-off current ratio is an essential requirement for the selector, therefore [5]. There are several types of selector devices, including the Mott type that are based on materials such as NbO_2 and VO_2 [6, 7], the diffusive or conductive bridge type that are based on metal ions diffusion in the dielectrics such as Ag in SiO_x [8], and the ovonic threshold switching occurred in chalcogenide materials such as GeSe and $GeAsTe_x$ [9, 10]. Amongst these candidates, OTS selectors have achieved fast switching speed in the order of ns, high ON-state current density larger than 20MA/cm^2, high half-bias nonlinearity larger than 10^5, and excellent endurance more than 10^{12} cycles [11-13].

Manuscript received MM/DD/2022. The review of this paper was arranged by Editor X. Y. This work was supported by the EPSRC of U.K. under Grants EP/M006727/1 and EP/S000259/1.

Z. Hu, W. Zhang (W.Zhang@ljmu.ac.uk), N. Saxena, P. Freitas, J. F. Zhang are with School of Engineering, Liverpool John Moores University, L3 3AF Liverpool, U.K. Z. Chai(zheng.chai@xjtu.edu.cn) is with the Center for Spintronics and Quantum Systems, and School of Materials Science and Engineering, Xi'an Jiaotong University, Xi'an 710049, China, also with the Peng Cheng Laboratory, Shenzhen 518055, China, and the Pazhou Laboratory (Huangpu), Guangzhou 510555, China. R. Degraeve, D. Garbin, A. Fantini, T. Ravsher, S. Clima, R. Delhougne L. Goux, and G.S.Kar are with IMEC, 3001 Leuven, Belgium.

The switching process in OTS has been described by different models, including the earlier thermally induced instability model [14], the electronic injection induced space charge model [15], the impact ionization induced generation and recombination model [16], the thermally assisted charge hopping model [16], the field induced nucleation model [17], and more recently, the electric field induced local bond modification models [18-21]. In the latest models, the defects transition from the ground state to the excited state at a high field due to the local bonds modification, and become delocalized. Hence the defect clusters are formed, which lead to the off-to-on switching. Vice-versa for the on-to-off switching at a low electric field, where the local bonds configuration recovered, and the defects return to ground state and become localized again [19].

Furthermore, the operation of 1S1Rs in which the selector is connected with a series resistor (Rs) were also investigated [22, 23], and it was suggested that the Rs plays an important role in the switching-on and switching-off process. For example, it was found that Rs defines the load line for the selector and hence its operation points and the holding current. Therefore, the selector is either switching volatilely between the static off-state and on-state, or oscillating in the transitional negative-differential-resistance (NDR) state [24-27]. Despite these early efforts, detailed experimental evidence is still lacking for characterizing the fast and sharp switching process in modern OTS devices. For example, it is not clear how the switching process and parameters in nanoscale OTS devices are affected by the series resistance, and what are the corresponding OTS switching mechanisms and kinetics. This missing information is important for understanding the operation of the 1S1R circuit and its modelling.

In this paper, several new observations in the GeAsTe OTS switching are investigated, including the different non-linear ON regions in OTS, and two distinct mechanisms of OTS switch-off: (1) the OTS switches off at zero total impedance of 1S1Rs when the Rs value is small, and (2) it switches off at the minimum OTS current when Rs is large. It is found that the switching process is associated with the defect cluster shrinking kinetics, which becomes Rs independent after the normalization. On the other hand, the rupture criteria of the defect cluster are dependent on Rs. Significant impact of Rs on the 1S1Rs operations and parameters are also identified. The paper is organized as follows. The device and experiments will be described in Section II, and the above observations and investigations will be discussed in Section III.

II. DEVICES AND EXPERIMENTS

A 20nm amorphous GeAsTe chalcogenide film is deposited by room temperature physical vapor deposition (PVD) and passivated with a low-temperature BEOL process. The TiN/GeAsTe/TiN selector uses a pillar (TiN) bottom electrode that defines the device size down to 50 nm, and integrates with a serial resistor Rs in the range of 1.8 kΩ to 400 kΩ in a 300 mm process flow, as shown in Fig.1a [28]. The I-V characterization was carried out by using a Keithley

4200A semiconductor analyzer either with the SMU for DC sweep, or with the embedded 4225-PMU ultrafast I-V module for pulse sweep. The probe station setup has a bandwidth of about 100MHz. An oscilloscope with high sampling rate of 1GS/s is also used to detect the ultra-fast oscillation in some of the tests. From a typical DC I-V of the 1S1R measured by a triangular pulse (**Fig. 1b**), the OTS-only I-V can be obtained by subtracting the voltage across the series Rs, $V_{OTS}=V_{1S1R}$-I·Rs, since the linear I-V at ON-state is dominated by Rs. As illustrated in **Fig.2a**, V_{th} is the threshold voltage for off-to-on switching, V_{hold} is the voltage where the on-to-off switching occurs. Note that these values are different for 1S1R and OTS-only. The threshold current and holding current, on the other hand, are the same for 1S1R and OTS-only due to the series connection. The I-V curves with various Rs values are shown in **Fig. 2b** for the 1S1Rs, and in **Fig. 2c** for the extracted OTS-only, respectively. The larger Rs value leads to lower on-state and holding current, higher threshold and holding voltage for the 1S1Rs. On the other hand, the OTS-only I-Vs in **Fig. 2c** follow a similar trajectory during the switching off process, demonstrating the validity of this extraction method, as the OTS in these devices have the same configuration and parameters. Despite this agreement, it will be demonstrated and explained in Section III that the OTS-only threshold voltage and holding voltage are affected by the Rs values.

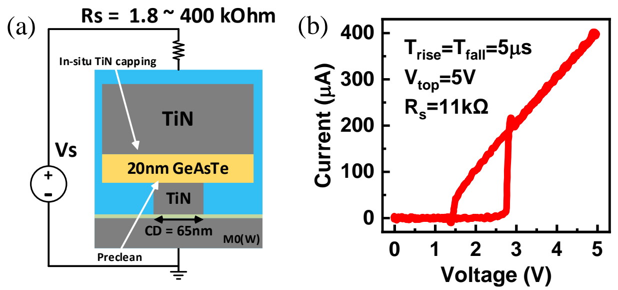

Fig. 1 (a) Illustration of the OTS structure in series with a resistor Rs. (b) A typical I-V of 1S1Rs measured by a triangular pulse. Pulse conditions and Rs value are labelled. Device size (CD) is 65nm unless specified otherwise.

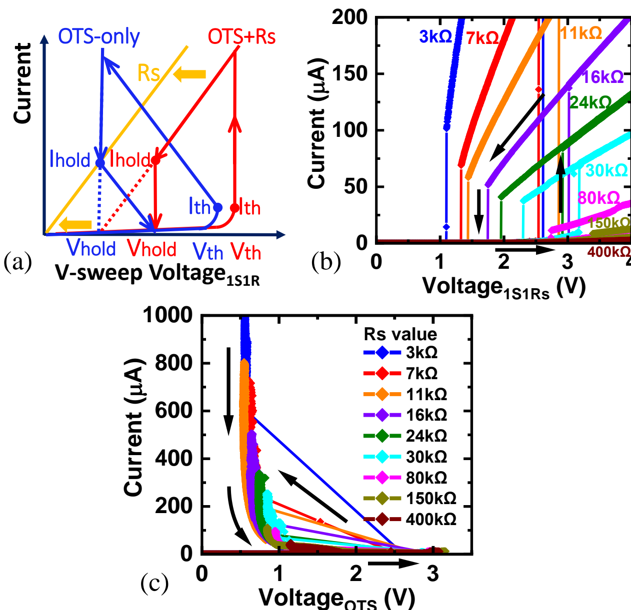

Fig. 2 (a) Illustration of OTS-only I-V extraction by $V_{OTS}=V_{1S1R}$-I·Rs. (b) I-V during DC voltage sweep measured for 1S1Rs with 3kΩ ≤Rs ≤ 400kΩ, and (c) the extracted I-V for OTS-only by the steps in (a).

III. RESULTS AND DISCUSSIONS

A. New observations in OTS-only I-V with different Rs

Further detailed inspection on the OTS-only I-V curves can reveal more significant differences in the switching process. For smaller Rs values in the range below 30 kΩ, the I-V curves largely follow the same trajectory, as shown in **Fig. 2c**, agreeing with previous results [28]. However, as shown in **Fig.3a**, for larger Rs values at and above 80 kΩ, a significant non-linear ON state (NL-ON) region is observed, for the first time, before the OTS switches to the OFF state, which deviates from the linear ON state that is defined by the Rs value. The origin of this NL-ON region needs to be investigated, as it could cause large errors if the Rs values in the 1S1Rs structure are read out from the current measured within this region. To rule out the possible contribution to this non-linear deviation from the test methods and speed, the results of DC voltage sweep, DC current sweep, and pulse voltage sweep with Rs = 80 kΩ are compared in **Fig. 3b**. The NL-ON region is observed and overlaps in all three cases, and similar results are also observed at other Rs values larger than 80kΩ (not shown). This confirms that the NL-ON is not caused by the test methods or test speed used in our measurements, hence the instrument settings and the RC effects in the probe and cable connections are not responsible for the occurrence of NL-ON.

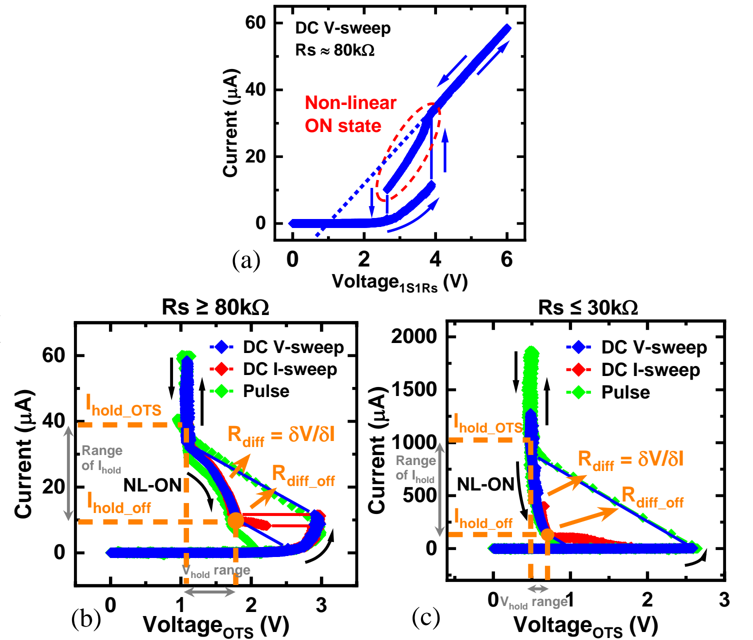

Fig. 3 (a) A significant non-linear ON state (NL-ON) region is observed before the OTS switches to OFF state with Rs≈80 kΩ. (b) Good agreement is observed in DC V-sweep, DC I-sweep, and pulse V-sweep when Rs=80 kΩ, all showing the NL-ON that overlap with each other during switch-off. It also overlaps with a part of switch-on sweep. This supports that NL-ON is not caused by the measurement speed in our setup. (c) A subtle NL-ON region is observed when Rs≲30 kΩ in DC V-sweep, DC I-sweep, and pulse V-sweep (Rs≈3kΩ for example) with good agreement in all cases. Definition of V_{hold_OTS}, I_{hold_OTS}, V_{hold_off} and I_{hold_off} and their ranges for OTS-only are also shown in (b) when Rs≳80kΩ, and (c) when Rs≲30kΩ.

It is well known that the OTS device exhibits a negative differential resistance region during the switching process, as evident in **Fig. 3b**. For the off-to-on voltage sweeps, the OTS current increases abruptly at V_{th}, and reaches the ON state at near the top end of, and in some cases

just within, the NL-ON region. For the on-to-off voltage sweeps, the OTS goes through the NL-ON region as the current reduces, until it reaches the holding point where the device switches off abruptly. The negative differential resistance in the large NL-ON region in Fig. 3b can be clearly seen, where $dV_{OTS}/dI_{OTS} < 0$. This large NL-ON region has not been reported in previous works [28, 29]. For the DC current sweep, the OTS switches ON at the same V_{th} as in the voltage sweeps, but then goes through the NL-ON region in both the off-to-on and on-to-off switching processes, which overlap in most of the NL-ON region. This is because the OTS current is step-controlled by the instrument during the current sweep, so that the abrupt changes can only be observed in the OTS voltage instead. The discrepancy in the small switching-off region after the holding point in Figs. 3b can be attributed to the differences in the test methods [24, 25].

In contrast, when Rs is smaller than 80 kΩ, a much subtler NL-ON region is observed, as shown in Fig. 3c for Rs =3 kΩ, where the subtler NL-ON only slightly deviates from the linear ON region. The DC voltage sweep also overlaps with the DC current sweep and the pulse voltage sweep. This confirms that the significant difference between Fig. 3b and Fig. 3c in the OTS switching off process can only be caused by the difference in Rs values. A part of the UP traces when reaching the ON state also falls within the NL-ON region and overlap with the DOWN traces during both the I-sweep & V-sweep, as shown in Figs. 3b&3c, suggests that the NL-ON is a common feature for both the switch-on and -off processes.

B. Correlation between NL-ON and NDR oscillation

The static and dynamic behavior of the 1S1R circuit has been analyzed as a dynamic system in previous works, by solving the circuit equations with the Kirchhoff Law [27]. When the OTS has negative differential resistance and is connected in series with a resistor, a stable state is obtained only if the differential resistance of the complete circuit is positive [27], and the effects of the series resistor can be analyzed as the load line for the OTS [24]. As illustrated in Fig. 4, Rs defines the load line for the OTS, and its interception with the OTS-only I-V defines the static operation point of the 1S1R. When the interception occurs in the NDR region, a relaxation oscillation will occur, as shown in refs. [26]. This oscillation can be explained briefly as follows. A spike of current increases within the NDR will result in a voltage reduction across the OTS, which in turn will lead to further current increase. This positive feedback loop causes the bias point to move along the NDR region until it reaches the V_{th} or V_{hold}, and the oscillation occurs between these two voltage levels. It was also reported that when the interception occurs near the top end of the NDR region (Fig.4b) where the total impedance has a positive value, the system will exhibit initial oscillations. It will then be dampened, leading to the stable state at the interception point in the 1S1R I-V, where $R_{diff,\ total} = Rs + dV_{OTS}/dI_{OTS} > 0$. $R_{diff_OTS} = dV_{OTS}/dI_{OTS} < 0$ can be extracted from the OTS-only I-V.

To further examine the potential impact of relaxation and dampened oscillation on the results in Fig. 3, an oscilloscope with a high sampling rate of 400M or 1G samples/s is used to detect if any oscillation occurs during the I-V sweeps. The oscilloscope has a 50-ohm internal impedance and is connected in series with the bottom electrode of the 1S1R, so that the current and voltage of the 1S1R can be extracted. As shown in Fig. 5a, when Rs≤30 kΩ, large oscillations can be observed within the NDR region during the DC I-sweep by the oscilloscope. The oscillation frequency is in the range of 100 kHz, as shown in the inset of Fig. 5a, which is defined by the total resistance and parasitic capacitance in the device and the measurement setup. For Rs≥80 kΩ, as shown in Fig. 5b, however, there is no oscillation being observed in the NL-ON region during the DC I-sweep, nor during the DC V-sweep. Oscillations can be observed only in a small region as shown in the inset of Fig. 5b, which is outside the NL-ON region and falls within the NDR region of the switching-off process. This suggests that for the quasi-DC measurement, the I-V characteristics in the NL-ON region in our measurements are the true representation of the static operation points of the 1S1R circuit without oscillations, and the NL-ON region in OTS-only I-V is determined by the differential resistance of the OTS, since the series resistance has been subtracted.

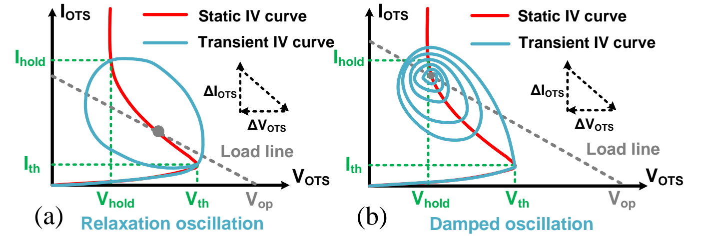

Fig. 4 Illustration of oscillation occurring if the OTS's operation point is within the NDR region under certain Rs values or at a constant current (e.g., at the grey dot). Relaxation (a) and dampened (b) oscillations may occur as illustrated by the blue lines, depending on the location of the interception point with the load line, when the total impedance of 1S1R, $R_{diff,\ total} = Rs + dV_{OTS}/dI_{OTS}$, is (a) negative or (b) positive, respectively.

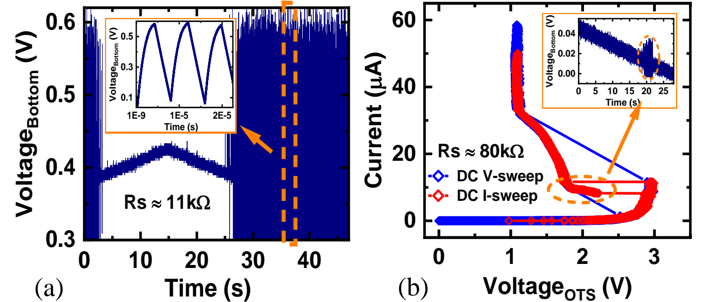

Fig. 5(a) Oscillations occur in NDR during switch-off in I-sweep when Rs⩽30kΩ, (b) but it only occurs in a smaller region when Rs≥80kΩ during the switching-off but not in the NL-ON region. Data are measured with an oscilloscope at 400M samples/s.

To further examine the oscillations during the pulse measurement, the OTS current signals recorded by the oscilloscope during the pulse voltage sweeping are shown in Figs. 6a&b, for Rs=11 kΩ and 80kΩ, respectively. For Rs= 80kΩ, the waveform is further modified so that the OTS is kept at different bias levels within the NL-ON region during switching-off, for 100 μs at each bias on the falling pulse edge. It is clear that there is no oscillation during the pulse voltage sweeps in both cases. Therefore, for the test conditions used in these measurements, neither the relaxation oscillation nor the dampened oscillation can be observed, confirming that the NL-ON is a true phenomenon associated with different Rs values.

C. Characterization of the switch-off process

As described in the latest models, the defects return from the delocalized excited state to the localized ground state during the switching-off process, so that the conductivity of OTS decreases. From the analysis in the previous sub-sections, this process starts

whilst the OTS is still at ON-state and its negative differential resistance increases when the electric field is getting smaller. To characterize the NL-ON region in the switching-off process, $R_{diff_OTS} = \delta V_{OTS}/\delta I_{OTS}$ is defined as the dynamic differential resistance of OTS-only, as shown in Figs. 3b&c, with smaller and larger Rs values, respectively. R_{diff_OTS} is negligible in the linear ON state, where the linear I-V is dominated by Rs. The I-V curves enter the NL-ON at (I_{hold_OTS}, V_{hold_OTS}), where the increase of $|R_{diff_OTS}|$ is no longer negligible in comparison to Rs, due to the defect clusters shrinking with the decreasing current [19]. The OTS switches off at (I_{hold_off}, V_{hold_off}) when the defect clusters rupture, and this is the OTS holding point commonly used for 1S1R [18, 19, 29], where $R_{diff_OTS} = R_{diff_off}$. The switching-off process is clearly different for Rs≤30 kΩ and Rs≥80 kΩ as Fig. 3 shows, indicating it is controlled by different mechanisms.

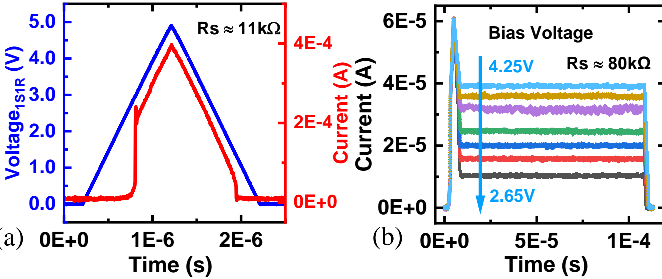

Fig. 6 There is no oscillation during V-sweep for (a) pulse or (b) quasi-DC tests with all Rs values (e.g., 11 kΩ and 80kΩ). Results in Fig. 6a are measured with an oscilloscope at 1G samples/s, and Fig.6b is measured with Keithley 4200 at 66M samples/s.

The impact of Rs on the boundary condition of the NL-ON region, i.e., (I_{hold_OTS}, V_{hold_OTS}) and (I_{hold_off}, V_{hold_off}), is further examined. Fig. 7a shows that I_{hold_OTS} decreases inversely with Rs, agreeing with previous works that it follows a linear line in the log-log scale [25]. (I_{hold_OTS}, V_{hold_OTS}) is the on-set point of defect cluster shrinking in the OTS when the differential resistance of OTS starts to become negative. Since the total differential resistance is dominated by Rs at this point, the inverse relation between I_{hold_OTS} and Rs is expected, as the OTS operates with Rs as the load. I_{hold_off} also decreases inversely when Rs is small (Rs ≤ 30kΩ), as expected. But for larger Rs values (Rs ≥ 80kΩ), I_{hold_off} no longer decreases with Rs and remains at a constant minimum value just below 10 μA. This provides clear evidence that there are two distinct switching-off mechanisms, associated with small and large Rs values, respectively. As shown in Fig.7b, for the smaller Rs, OTS switches off when $|R_{diff_OTS}|$ reaches Rs (≤30 kΩ), where the total impedance of the 1S1Rs circuit, $Rs+R_{diff_OTS}$, becomes 0 (inset of Fig.7b). For larger Rs, the maximum value of $|R_{diff_OTS}|$, $|R_{diff_max}|$, becomes saturated at ~40kΩ and can no longer reach Rs (80kΩ-400kΩ), hence the total impedance of 1S1Rs remains positive. The OTS current must decrease to a minimum holding level to trigger the switch-off, as shown in Figs. 7a.

This is further confirmed by normalizing each of the I-V curves in the three different methods as shown below, so that the trajectory of the switching-off kinetics with various Rs can be compared directly:

(1) Shift and align each I-V at V_{hold_OTS}, as shown in Fig.8a. This method is used to remove the changes in the V_{hold_OTS} value that are caused by Rs (which will be discussed later), so that the kinetics of switching-off at various Rs can be compared. It is clear in Fig.8a that the OTS switches off at different absolute current levels with various Rs, as the I_{hold_OTS} changes from >1mA to the level of 10 μA, supporting that the reducing electric field should be the main factor controlling the switching-off process, instead of the current or power, as shown in our previous modelling work [19].

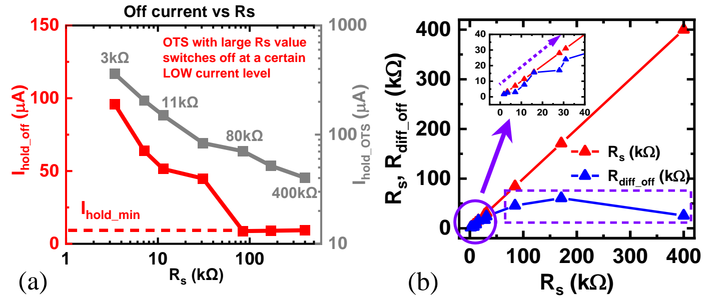

Fig. 7(a) I_{hold_OTS} and I_{hold_off} vs Rs for OTS-only. I_{hold_OTS} decreases inversely with Rs. OTS switches OFF at a common I_{hold_min} when 80kΩ ≤Rs≤400kΩ. (b) R_{diff_off} is plotted vs Rs. For smaller Rs (inset), OTS switches off when $Rs+R_{diff_OTS}=0$. For larger Rs, the maximum R_{diff_OTS} is less than 50 kΩ. OTS switches OFF when it reaches the minimum I_{hold} with Rs>80 kΩ.

(2) Normalize each I_{OTS} value by its own I_{hold_OTS} as shown in Fig. 8b. This method is used to account for the relative change in I_{OTS} only, so that the trajectory of the switching-off kinetics can be compared despite the large differences in the absolute current values caused by various Rs. It then appears that there are two distinct groups of I-V curves, for the smaller and larger Rs values, respectively. The group with smaller Rs values follows a similar trajectory and has the subtler NL-ON region. The group with larger Rs values exhibits the significant NL-ON and switches off at a higher V_{hold_off}. Hence the relative changes in current, $\Delta I_{OTS}/I_{OTS}$, or in voltage, ΔV_{OTS}, may not be the only or dominant factor triggering the switch-off. The impedance value should play the most significant role, instead.

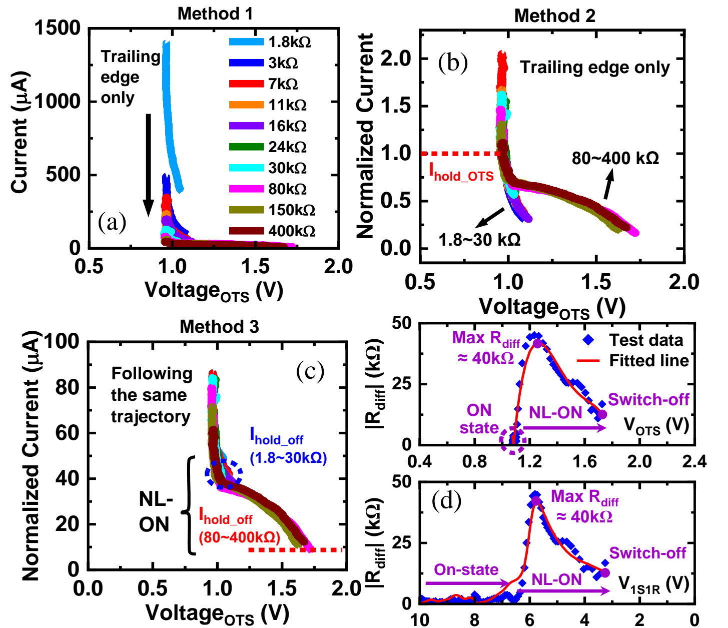

Fig.8 Normalization of each I-V at various Rs by 3 methods: (a) shift and align each I-V at V_{hold_OTS}; (b) normalize each I_{OTS} by its own I_{hold_OTS} to account for the relative change in I_{OTS} only; (c) normalize each I_{OTS} by the current ratio between that at its own R_{diff_off} vs that at $R_{diff_OTS}(80k\Omega)$ where $R_{diff_OTS}(80k\Omega) = R_{diff_off}(Rs)$. All curves follow the same shape after the normalization, suggesting that the trajectory is determined by R_{diff}. i.e., the defect cluster dynamics in OTS. (d) the inverse of the slope of the curves in (c) show a peak in the middle of the NL-ON region, against V_{OTS} and V_{1S1R}, respectively. This curve can be used to estimate the kinetics of defect cluster shrinking.

(3) Normalize each I-V curve by the R_{diff_OTS} on the reference I-V curve of Rs=80kΩ instead, so that the impact of R_{diff_OTS} on switching-off kinetics can be compared. This is done by extracting the R_{diff_off} value at the switching-off point on each I-V curve in Fig.8a, and then finding the corresponding point on the reference I-V curve of 80kΩ where $R_{diff_OTS}(80k\Omega) = R_{diff_off}(Rs)$. The y-axis of I-V(Rs) is then rescaled by the ratio of the currents at these two points, so that these two current levels become overlapped after the normalization. All curves after this normalization are then found following the same trajectory, as shown in Fig. 8c, suggesting that the shape of the normalized I-V curves in the NL-ON region is determined by R_{diff_OTS}. This supports that the trajectory in the switching-off process is caused by the dynamic differential resistance of the OTS, from which the kinetics and impact of the defect cluster modulation may be estimated. As shown in Fig. 8d, the inverse of the slopes of these normalized curves has a peak in the middle of the NL-ON region, where the R_{diff_OTS} reaches the maximum value, for both the OTS-only and the 1S1R operations. Hence the shrinking speed of the defect cluster accelerates at the beginning of NL-ON. After the peak is reached, the speed starts to reduce as the current decreases further, and eventually the clusters rupture at the minimum current for Rs≥80kΩ.

After the above normalization, it is observed in Fig.9a that both I_{OTS} and V_{OTS} show two regions in the NL-ON range, (I_{hold_OTS} - I_{hold_off}) and (V_{hold_off} - V_{hold_OTS}), in its Rs dependence. One is from ~2kΩ to 30 kΩ. This is the region that $|R_{diff_OTS}|$ can become large enough to reach the smaller Rs value, in which both I_{hold_off} and V_{hold_off} change slightly; The other one is from 80kΩ to 400kΩ, where the OTS switches off at the same I_{hold_min} level and at a much larger V_{hold_off}. Hence the full OTS switch-off characteristics and two different switch-off mechanisms can be revealed and explained as follows.

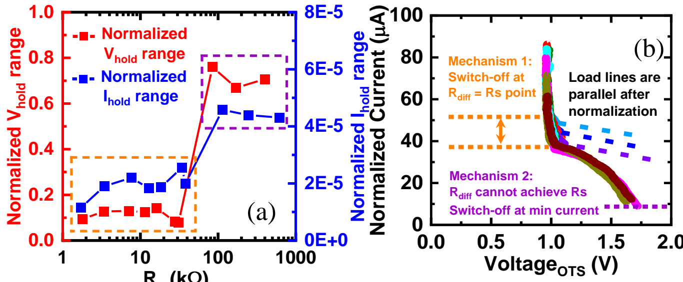

Fig.9 (a) Rs dependence of the normalized NL-ON range, (I_{hold_OTS}-I_{hold_off}) and (V_{hold_off} -V_{hold_OTS}). (b) The normalized data, with the load lines at the switching-off points for Rs≤ 30kΩ. The two distinct switching-off regions and its dependance on Rs values is clearly shown. The OTS switches off when $|R_{diff_OTS}|$ reaches the Rs (≤30kΩ). Once the maximum $|R_{diff_OTS}|$ cannot exceed the Rs, the OTS will switch-off at the minimum current level.

The above observation agrees in principle with our previous defect clusters model for OTS with a field and current dependent transition dynamics, modelled by Monte Carlo simulation and the spectroscopic technique [19]. When the OTS current reduces, the defect clusters start to shrink, and the defect number in the clusters reduces, so that $|R_{diff_OTS}|$ increases and V_{OTS} increases. When $|R_{diff_OTS}|$ reaches the Rs (≤30kΩ), the total impedance of 1S1Rs becomes 0 and the OTS is out of equilibrium and switches OFF at V_{hold_off}. As shown in Fig. 9b, the OTS switches off at different points when R_{diff_OTS} reaches Rs, where their load lines become parallel after the normalization by R_{diff_OTS} as shown in method (3), supporting the switching-off mechanism of R_{diff_OTS} + Rs=0. For larger Rs (≥80kΩ), the maximum $|R_{diff_OTS}|$ value can no longer reach Rs, the OTS is forced to operate at NL-ON state in a low current regime, where I_{OTS} keeps decreasing until it is below the minimum OTS holding current, then the conductive cluster is broken and the OTS switches OFF [19], as illustrated in Fig. 9b. Hence the I-V trajectory in the NL-ON is determined by the defect clusters shrinking kinetics in the OTS.

The NL-ON, especially when Rs ≥ 80kΩ, will lead to large errors when reading the memory element of large R values, as shown in Fig.3a. It is also found that both the V_{th_OTS} and V_{hold_OTS} increase with Rs values, as shown in Fig. 10. This agrees with the increase of V_{th_OTS} with Rs values observed in [18], which was attributed to the weaker defect clusters caused by the smaller OTS operation currents with larger Rs values. Hence the OTS-only V_{th_OTS} and V_{hold_OTS} also contribute to the total ΔV_{th} & ΔV_{hold} in 1S1R operation, in addition to that caused by the programmable R value in the non-volatile memory,

$$\Delta V_{th}(Rs)=\Delta V_{th_OTS}(Rs)+\Delta V_{th_Rs} \quad (1)$$
$$\Delta V_{hold}(Rs)=\Delta V_{hold_OTS}(Rs)+\Delta V_{hold_Rs} \quad (2)$$

where ΔV_{th_Rs} and ΔV_{hold_Rs} are induced by Rs itself, $\Delta V_{th_OTS}(Rs)$ and $\Delta V_{hold_OTS}(Rs)$ are induced by OTS. These large Rs dependence of V_{th_OTS} and V_{hold_OTS} should be accounted for in the 1S1R circuit simulation and analysis, therefore. Future work is needed to further investigate the defect cluster shrinking kinetics in the OTS, and to implement the observed relations between NL-ON, ΔV_{th_OTS}, ΔV_{hold_OTS} and Rs into the modelling of 1S1R operations for accurate extraction of both ΔR and $\Delta V_{th}/\Delta V_{hold}$ in memory cell.

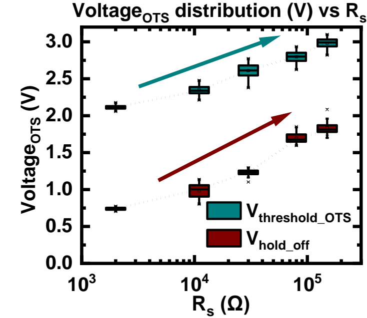

Fig.10 V_{th_OTS} and V_{hold_off} vs Rs for OTS-only without normalization. Both increase with Rs values, which contribute to the total ΔV_{th} and ΔV_{hold} in 1S1R operation, in addition to that caused by the programmable R value in the memory element.

IV. Conclusions

Experimental evidence in this work shed new insights into the full switching-off process of GeAsTe OTS and its dependence on the series resistance value. When the Rs is small, the OTS switches off when the total differential resistance reaches zero. When the Rs value is large, the OTS switches off at a constant minimum OTS holding current level. The changes in $|R_{diff_OTS}|$ during the switching-off process can be attributed to the defect cluster shrinking kinetics in the OTS and can be therefore measured and characterized. The resulted non-linear ON-state region and the dependence of OTS-only threshold volage and holding voltage on the resistance level of the memory element have a significant impact on the parameter extraction and simulation of 1S1R operation. Future work is needed to fully understand the defect cluster shrinking kinetics, to further model and simulate its impact.

REFERENCES

[1] G. W. Burr *et al.*, "Access devices for 3D crosspoint memory," *Journal of Vacuum Science & Technology B, Nanotechnology and Microelectronics: Materials, Processing, Measurement, and Phenomena,* vol. 32, no. 4, p. 040802, 2014.

[2] J. T. Zhou, K. H. Kim, and W. Lu, "Crossbar RRAM Arrays: Selector Device Requirements During Read Operation," *IEEE Transactions on Electron Devices,* vol. 61, no. 5, pp. 1369-1376, May 2014, doi: 10.1109/Ted.2014.2310200.

[3] H. Cheng *et al.*, "Ultra-high endurance and low I OFF selector based on AsSeGe chalcogenides for wide memory window 3D stackable crosspoint memory," in *2018 IEEE International Electron Devices Meeting (IEDM)*, 2018: IEEE, pp. 37.3. 1-37.3. 4.

[4] D. A. Robayo *et al.*, "Integration of OTS based back-end selector with HfO2 OxRAM for crossbar arrays," in *2019 IEEE 11th International Memory Workshop (IMW)*, 2019: IEEE, pp. 1-4, doi: 10.1109/IMW.2019.8739746.

[5] S. Jia *et al.*, "Ultrahigh drive current and large selectivity in GeS selector," *Nat Commun,* vol. 11, no. 1, p. 4636, Sep 15 2020, doi: 10.1038/s41467-020-18382-z.

[6] E. Cha, J. Park, J. Woo, D. Lee, A. Prakash, and H. Hwang, "Comprehensive scaling study of NbO2 insulator-metal-transition selector for cross point array application," *Applied Physics Letters,* vol. 108, no. 15, p. 153502, Apr 11 2016, doi: 10.1063/1.4945367.

[7] M. Son *et al.*, "Excellent Selector Characteristics of Nanoscale VO2 for High-Density Bipolar ReRAM Applications," *IEEE Electron Device Letters,* vol. 32, no. 11, pp. 1579-1581, Nov 2011, doi: 10.1109/Led.2011.2163697.

[8] J. Yoo, J. Woo, J. Song, and H. Hwang, "Threshold switching behavior of Ag-Si based selector device and hydrogen doping effect on its characteristics," *Aip Advances,* vol. 5, no. 12, p. 127221, Dec 2015, doi: 10.1063/1.4938548.

[9] Z. Chai *et al.*, "Stochastic Computing Based on Volatile GeSe Ovonic Threshold Switching Selectors," *IEEE Electron Device Letters,* vol. 41, no. 10, pp. 1496-1499, Oct 2020, doi: 10.1109/Led.2020.3017095.

[10] Z. Chai *et al.*, "Cycling Induced Metastable Degradation in GeSe Ovonic Threshold Switching Selector," *IEEE Electron Device Letters,* vol. 42, no. 10, pp. 1448-1451, Oct 2021, doi: 10.1109/Led.2021.3109582.

[11] Y. Koo, K. Baek, and H. Hwang, "Te-based amorphous binary OTS device with excellent selector characteristics for x-point memory applications," in *2016 IEEE Symposium on VLSI Technology*, 2016: IEEE, pp. 1-2, doi: 10.1109/VLSIT.2016.7573389.

[12] B. Govoreanu *et al.*, "Thermally stable integrated Se-based OTS selectors with >20 MA/cm2 current drive,> 3.10 3 half-bias nonlinearity, tunable threshold voltage and excellent endurance," in *2017 Symposium on VLSI Technology*, 2017: IEEE, pp. T92-T93, doi: 10.23919/VLSIT.2017.7998207.

[13] F. Hatem *et al.*, "Endurance improvement of more than five orders in GexSe1-xOTS selectors by using a novel refreshing program scheme," *Int El Devices Meet,* 2019. [Online]. Available: <Go to ISI>://WOS:000553550000018.

[14] D. Eaton, "Electrical Conduction Anomaly of Semiconducting Glasses in the System As—Te—I," *Journal of the American Ceramic Society,* vol. 47, no. 11, pp. 554-558, 1964, doi: 10.1111/j.1151-2916.1964.tb13816.x.

[15] N. Mott, "Conduction in non-crystalline systems: VII. Non-ohmic behaviour and switching," *Philosophical Magazine,* vol. 24, no. 190, pp. 911-934, 1971, doi: 10.1080/14786437108217058.

[16] D. Adler, M. S. Shur, M. Silver, and S. R. Ovshinsky, "Threshold Switching in Chalcogenide-Glass Thin-Films," *Journal of Applied Physics,* vol. 51, no. 6, pp. 3289-3309, 1980, doi: 10.1063/1.328036.

[17] V. G. Karpov, Y. A. Kryukov, S. D. Savransky, and I. V. Karpov, "Nucleation switching in phase change memory," *Applied Physics Letters,* vol. 90, no. 12, p. 123504, Mar 19 2007, doi: 10.1063/1.2715024.

[18] S. Kabuyanagi *et al.*, "Understanding of tunable selector performance in Si-Ge-As-Se OTS devices by extended percolation cluster model considering operation scheme and material design," in *2020 IEEE Symposium on VLSI Technology*, 2020: IEEE, pp. 1-2, doi: 10.1109/VLSITechnology18217.2020.9265011.

[19] R. Degraeve *et al.*, "Modeling and spectroscopy of ovonic threshold switching defects," in *2021 IEEE International Reliability Physics Symposium (IRPS)*, 2021: IEEE, pp. 1-5.

[20] S. Clima *et al.*, "Ovonic Threshold-Switching GexSey Chalcogenide Materials: Stoichiometry, Trap Nature, and Material Relaxation from First Principles," *Physica Status Solidi-Rapid Research Letters,* vol. 14, no. 5, p. 1900672, May 2020, doi: 10.1002/pssr.201900672.

[21] P. Noe *et al.*, "Toward ultimate nonvolatile resistive memories: The mechanism behind ovonic threshold switching revealed," *Sci Adv,* vol. 6, no. 9, p. eaay2830, Feb 2020, doi: 10.1126/sciadv.aay2830.

[22] J. M. Lopez *et al.*, "Ge-Se-Sb-N-based OTS scaling perspectives for high-density 1S1R crossbar arrays," in *2021 IEEE International Memory Workshop (IMW)*, 2021: IEEE, pp. 1-4, doi: 10.1109/IMW51353.2021.9439606.

[23] C. Wu *et al.*, "Low-voltage (~ 1.3 V), Arsenic Free Threshold Type Selector with Ultra High Endurance (> 10 11) for High Density 1S1R Memory Array," in *2021 Symposium on VLSI Technology*, 2021: IEEE, pp. 1-2.

[24] R. Pryor and H. Henisch, "Nature of the on-state in chalcogenide glass threshold switches," *Journal of Non-Crystalline Solids,* vol. 7, no. 2, pp. 181-191, 1972, doi: 10.1016/0022-3093(72)90288-8.

[25] A. J. Hughes, P. A. Holland, and A. H. Lettington, "Control of Holding Currents in Amorphous Threshold Switches," *Journal of Non-Crystalline Solids,* vol. 17, no. 1, pp. 89-99, 1975, doi: 10.1016/0022-3093(75)90116-7.

[26] Y. Yu, B. Zhao, J. M. Goodwill, Y. Ma, J. A. Bain, and M. Skowronski, "Electrical and Thermal Dynamics of Self-Oscillations in TaO x-Based Threshold Switching Devices," *ACS Applied Electronic Materials,* vol. 2, no. 3, pp. 683-691, 2020, doi: 10.1021/acsaelm.9b00782.

[27] S. Lavizzari, D. Ielmini, and A. L. Lacaita, "A New Transient Model for Recovery and Relaxation Oscillations in Phase-Change Memories," *IEEE Transactions on Electron Devices,* vol. 57, no. 8, pp. 1838-1845, Aug 2010, doi: 10.1109/Ted.2010.2050963.

[28] D. Garbin *et al.*, "Composition optimization and device understanding of Si-Ge-As-Te ovonic threshold switch selector with excellent endurance," in *2019 IEEE International Electron Devices Meeting (IEDM)*, 2019: IEEE, pp. 35.1. 1-35.1. 4, doi: 10.1109/IEDM19573.2019.8993547.

[29] W. Devulder *et al.*, "A combinatorial study of SiGeAsTe thin films for application as an Ovonic threshold switch selector," *Thin Solid Films,* vol. 753, p. 139278, 2022, doi: 10.1016/j.tsf.2022.139278.